Journal of Green Engineering (JGE)

Volume-10, Issue-12, December 2020

IoT based Automatic Detection of Glaucoma Disease in OCT and Fundus Images Using Deep Learning Techniques

[1]R. Anandh and [2]G. Indirani

[1]*Research Scholar, Department of CSE, FEAT, Annamalai University, Chidambaram, Tamil Nadu, India.*
E-mail: raanandh37@gmail.com
[2]*Associate Professor, Department of CSE, Government College of Engineering, (Deputed from Annamalai University) Bargur, Tamil Nadu, India.*
E-mail: induk0992@gmail.com

Abstract

Internet of Things (IoT) and cloud computing are two connected areas that rely on each other from which physicians track and assist remote patients. Successful treatment of diseases includes a model equipped with IoT for the identification of diseases. Computer-aided diagnostics are becoming more popular in all fields of pharmaceuticals, including ophthalmology, with the improvement of image recognition and effective machine learning techniques. This approach continue to offer systematic and effective large-scale testing of a range of picture methods to help medical professionals in the identification of diseases. Subsequently, the optic nerve is the maximum vital component of the retinal fundus picture for the diagnosis of glaucoma. This article suggests a two-phase structure that initially recognises and separates the optic disc and ultimately categorises it into glaucoma or stable. The initial step will focus on the RCNN (Regions with Convolutional Neural Network) and will be accountable for defining and isolating the optical nerve head from the retinal fundus signal. At the same time, deep learning strategies are used in the second process to categorise the mined disc into glaucoma or stable. In addition, a rule-based semi-automatic ground truth generation approach is also developed that provides important interpretations to train the RCNN-based model for automatic disc localization. Area under

Journal of Green Engineering, Vol. 10_12, 13621-13643.
© 2020 *Alpha Publishers. All rights reserved.*

the Receiver Operational Characteristic Curve is achieved for the classification of glaucoma equivalent to 0.874, which reflects a relative improvement of 2.7% over the recent results already observed for the classification of the ORIGA data set. For data sets without pre-determined test and training splits and with class disparity, the experimental assessment of the classification of glaucoma on ORIGA reveals that the exposure of AUC (Area Under the Curve) alone does not disclose an accurate picture of the performance of the classifier and calls for additional performance tests to validate the effects.

Keywords: IoT, Area Under the Curve, Regions with Convolutional Neural Network, Automatic Detection of Glaucoma Disease, Deep Learning Techniques.

1 Introduction

The WHO (World Health Organization) states that glaucoma is the next driving origin for visual impairment. In 2010, 60 million people were affected [1] and in 2020 about 70.6 million cases of vision disability will be affected [2]. Glaucoma is one of the primary causes of reduced vision in people under the age of 60. From now on, the timely position of glaucoma assumes the virtual role of capturing unrecoverable damage to the eyes. Especially for mature adults, the vision issue of glaucoma causes a long-term visual impairment. This hopeless problem of glaucoma is thus essentially understood in the early stages [3]. A few forms of glaucoma can be expressed as describes:

- Congenital glaucoma.
- normal-tension in glaucoma,
- the angle-closure of glaucoma, and
- Open-angle glaucoma [4].

In addition, there are important components to be tested before glaucoma is detected, such as pachymetry, gonioscopy, perimetry, tonometry and ophthalmoscopy. At this stage, the glaucoma diagnosis is done on the basis of the clinical record of the patient's ONH (optical nerve head) physical estimation, vision field failure measures, and IOP (intraocular pressure) by ophthalmoscopy [5]. Glaucoma assessment can be done by visual field error, OCT (optical coherence tomography), IOP measurement, ONH assessment, RNFL (retinal nerve fibre layer) and digital fundus camera [6].

IOP is increasingly expanding due to a deterioration of the waste configuration of the eyes. At that point, the weight of the fluid in the eyes rises constantly, causing damage to the optical disc of the eyes [7] and causing a permanent loss of vision [1], which causes the unrecoverable issue of glaucoma. In addition, the weakened RNFL decreases the texture of the RNFL, which is also one of the basic drivers of the problem of glaucoma [8-

9]. In addition, a few possible approaches give rise to glaucoma complications, such as visual field functional stoppage, nerve fibre plate, ONH, and at the same time simple adjustments [10].

1.1 Recognition of Glaucoma Utilizing Retinal Image

This section provides insights into the representation of the retinal fundus where the breadth of the RNFL [11] is used for the study of glaucoma. The important advantageous location of the retinal fundus images is that, in most medical cases, retinal fundus photos can be collected without any complications. Retinal picture is one of the main non-invasive techniques in the therapeutic territory for the diagnosis of glaucoma [11], which involves non-healthy and healthy retinas for ophthalmologists[12]. At that point, the removal of data from the computerised picture analysis is used to locate visual glaucoma infections[13].

Figure 1 shows the typical design of the glaucoma recognition measure using the retinal fundus graphic. The phases of glaucoma identification can be seen as defined in the following:

- Interpret the image input.
- On the basis of ROI extraction (area of interest), the path to testing, and channel selection, pre-process the input image.
- Segment input image, e.g. segmentation, optical disc detection and retinal vessel-based segmentation.
- Categorize the test area using segmentation.
- Mining the range of features and texture features and
- Categorize the input image using different classifiers, such as NB (naive Bayes) classifiers, SVM (support vector machine), ANN (artificial neural network) and KNN (k-nearest neighbour).

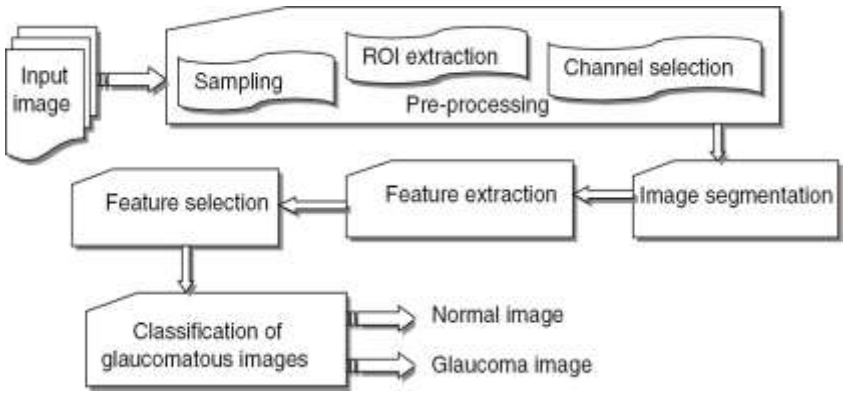

Figure 1 A Common Block Scheme of Recognition of Glaucoma Procedure Using Retinal Fundus Images

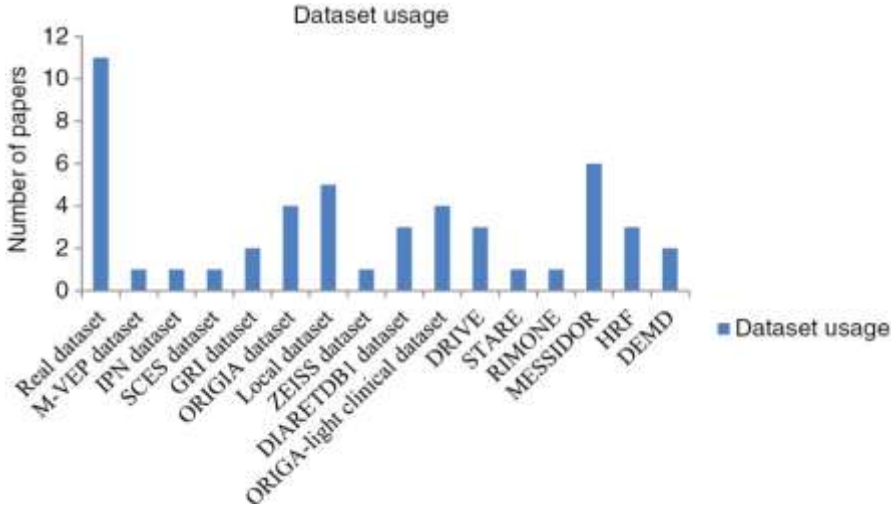

Figure 2 Bar Graph depends on the Used Data Set

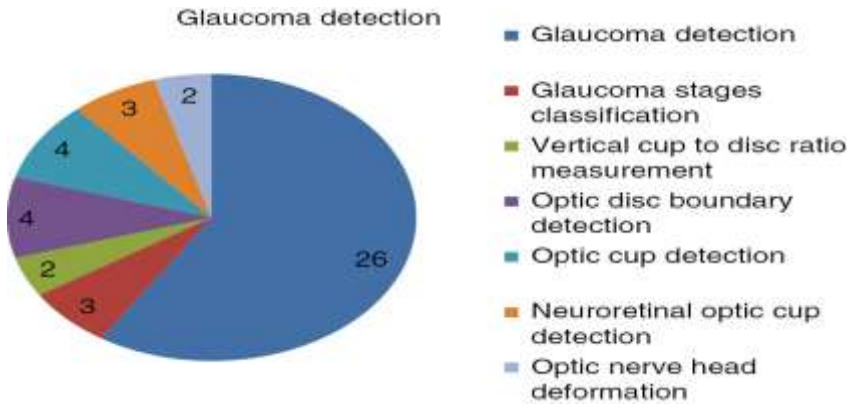

Figure 3 Glaucoma Detection through Various Techniques

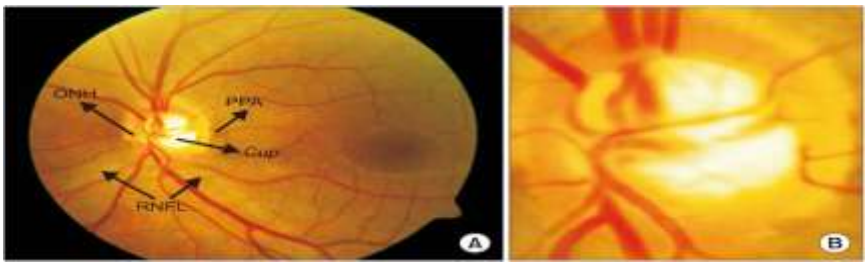

Figure 4 Models of the Original Image (A) and ROI (region of interest) Image of ONH (optic nerve head) (B). RNFL: Retinal Nerve Fiber Layer, PPA: Parapapillary Atrophy

Figure 2 shows Bar Graph depends on the Used Data Set. Figure 3 shows Glaucoma Detection through Various Techniques. Figure 4 shows Models of the Original Image (A) and ROI (region of interest) Image of ONH (optic nerve head) (B). RNFL: Retinal Nerve Fiber Layer, PPA: Parapapillary Atrophy

2 Methods

The full optical disc classification and localization technique is given in this segment, beginning with a brief summary of the portion of the image datasets of the retinal fundus that were used in this analysis. From this introduction, it appears to be seen that all of the following are the data sets generated for disc localization by every bouncing box ground truth and, subsequently, instigating the creation of the method of producing ground truth. Figure 5 shows Healthy Disc, Initial Glaucoma, Mild Glaucoma and Severe Glaucoma in Retinal Fundus.

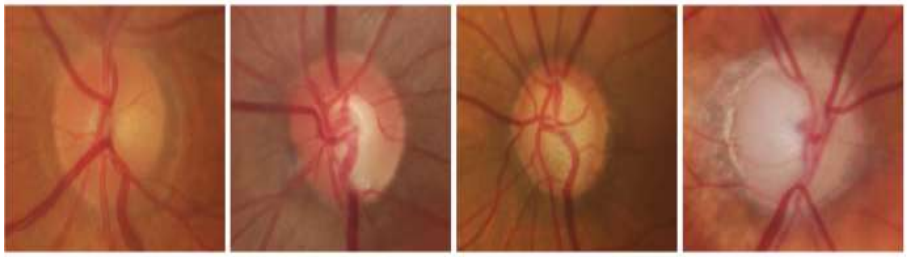

Figure 5 Healthy Disc, Initial Glaucoma, Mild Glaucoma and Severe Glaucoma in Retinal Fundus

3 Data sets utilized in this analysis

3.1 ORIGA

ORIGA [14] aims to provide the medical ground reality to target classification and segmentation algorithms. It also provides CDR and classifies any picture as stable or glaucoma. Custom app testing tool is used to build segmentation manually for OC and OD. This data set was used as a benchmark data set in some of the more recent contemporary glaucoma classification studies. The data collection was compiled by I1 and includes 168 glaucoma and 482 balanced images. ORIGA is otherwise known as the Online Retinal Fundus Glaucoma Review and Testing Image Website.

3.2 High-Resolution Fundus [15] (HRF)

The image archive is obtained from the Department of Ophthalmology, U1. It consists of 15 images with glaucoma and 15 images of diabetic retinal disorder and 15 balanced images. The gold standard (GS) and the binary vessel segmentation are provided for each image. The gold standard data is generated by a community of experts and physicians.

3.3 CFI & OCT

This data set [16] contains the Color Fundus Photographs and the OCT (Optical Coherence Tomography) of both eyes of 55 healthy people obtained at the Department of Ophthalmology of H1. Although the images have been seized as a portion of the macular contrast optical coherence tomography (OCT) study in the left and right eyes of common citizens, there is no ground-level reality regarding the OD location or segmentation of blood vessels or OD.

3.4 DIARETDB1 Standard

DIARETDB1 (DIAbetic RETinopathy DataBase Calibration Stage 1)[17] is a freely available data collection composed of 90 colour retinal fundus photographs taken at H2. The key purpose of this data collection is to standardise the overall performance of automated detection strategies for diabetic retinal disease. Five unbiased medical professionals are used to interpret the data collection to include patterns for haemorrhage, soft and heavy, and exudation of microaneurysms. According to the trends presented, 85 of the photographs had a moderate moderate, non-proliferating diabetic retinal disorder. Although the remaining 5 images have been observed to be solid. The data collection does not include retinal disease outcomes dependent on ground-level OD localization or ICDR (International Clinical Diabetic Retinopathy) degree of seriousness.

3.5 DRIVE

DRIVE (Digital Retinal Images for Vessel Extraction) [18] involves of 45 images collected in C1 as portion of the diabetic retinal disease examination database. Nor does this data collection contain some explanatory notes for the optical disc location. The data collection is split into test and train divisions. The test collection contained 23 images of two manually segmented masks. The instruction collection contains 22 photos of certain manual blood vessel segmentation masks.

3.6 DRIONS-DB

DRIONS-DB (Digital Retinal Images for Optical Nerve Segmentation DataBase)[19] is one of the data sets for the performance assessment of the ONH (Optic Nerve Head) segmentation of the retinal image. This data collection contains 110 photographs obtained by the Department of Ophthalmology at H2. It provides ONH forms followed by two different specialists using image interpretation tools.

3.7 Messidor

Messidor[20] is a massive, publicly available data set of 1,250 high-resolution colour fundus images. 450 photographs have been used in this data collection, which is obtained from three U1 ophthalmological departments. It offers a diabetic retinopathy rating of 3 (severe) from 0 (healthy) and a retinal edoema likelihood of 0 (no danger) to 2 (high risk) for each picture. This paper is initiated to categorise retinal fundus images into glaucoma and stable. It is also recognised as Methods for testing segmentation and indexing procedures in the area of retinal ophtalmology.

Although the entire retinal fundus image is fed to CNN, it does not support the network that concentrates on a large portion of the image, such as the OD, for the task of classification given. Subsequently, it was necessary to delete the ROI and forward it to the network. A brief analysis of disc localization methods showed that new approaches have been experimental and have been primarily designed for single or multiple data sets. Such approaches could not be summed up accurately on various data sets. There was a genuine need for a fully computed, hearty, and data collection of autonomous disc localization strategies that could be extended to multiple retinal fundus image data sets with high accuracy and reliability. Using the directed neural network paradigm, this was conceivable. The accessibility of the ground truth for training, however, included this method, which was not found in any of the seven data sets used in this analysis. It was then thought fitting to have initially invented a methodology for the ground reality era of negligible individual participation. Then the preparation is done with the ground reality generated and the presentation of a fully robotic disc localization technique is standardised.

The step-by-step progress from the formation of the GT to the mining of the disc and, in the end, the classification is deliberated in feature.

4 Semi-Automatic Processing of GT Creation for OD Localization

A heuristic technique for estimating the OD region is developed in the retinal photos. The results of this heuristic technique are physically evaluated and, where appropriate, essential changes are made. Figure 6 demonstrates the operating phase of this system. It contains of a heuristic calculation which provides a suggestion for the OD region, which is then physically tested by a specialist. So that the localization ground reality is generated for each of the seven data sets mentioned in the past field. The utility of the heuristic localization algorithm was evaluated by choosing three publicly available data sets of high-target retinal fundus shading photos. Table 1 includes a diagram of the data sets used. Out of 780 photos, 48 photos were taken for

clearance, and 525 were randomly selected for training, and the remaining 207 photos were saved for further research. The test set was used to explore various experimental limits such as the retinal edge of the crop edge and the most drastic scale of the legitimate disc spectrum and so on. These observational limits were selected physically with the overall aim of having the best acceptance precision. When certain characteristics are determined, they have been set during testing. To ensure that these characteristics chip away from pictures in different data sets for different priorities, all the photographs were resized to a static scale (1500×1500), primed the pictures, and then resized back to their specific size. The mixing of three separate data sets presents enough of the data set varieties in the images to approve the precision and strength of the heuristic technique together and thoroughly.

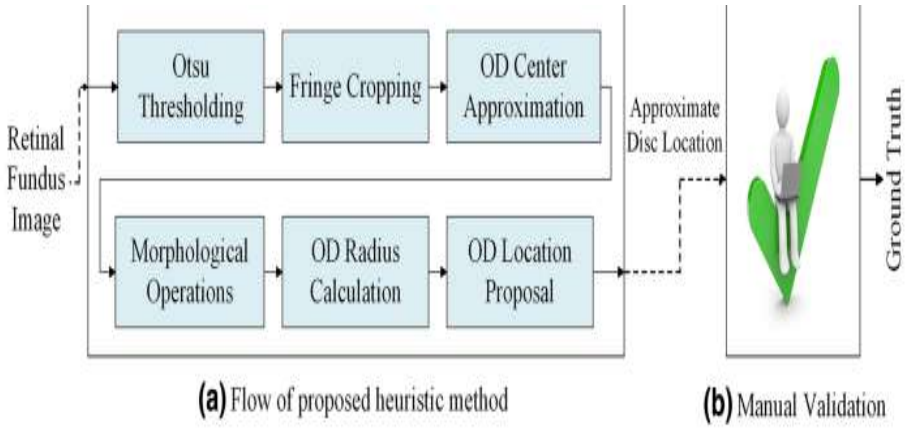

Figure 6 Work Processes of Semi-Automated Ground Truth Creation System

Table 1 Summary of Data Sets Utilized to Evaluate the Heuristic Technique

Data set	Overall size	Glaucoma	Healthy
CFI&OCT	100	-	100
HRF	30	15	15
ORIGA	650	168	482

5 Heuristic Algorithms for OD Localization

The proposed calculation for the exploration of the hypothesised OD area from retinal images was discussed in this segment. The main achievement of the strategy has been seen in the figure. It's around 6a. It appears from the

awareness that OD is typically the most brilliant part of the retinal fundus picture. In this case, there may be some lovely spots in the picture, due to some ill or deficient picture-taking circumstances that may influence the presence of any experimental or heuristic technique. Figure 7 provides two examples of this kind of false luminous spot. The key section of each subfigure displays the colour hue of the retinal fundus, and the next segment exposes a twofold picture proportional to the individual shading image.

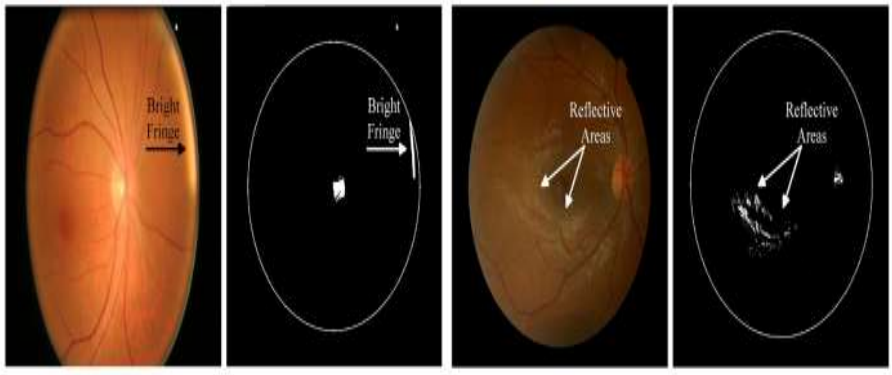

Figure 7 a) Binary Images Demonstrating Disingenuous Light Points. **b)** RGB Image is Scaling to Fit within the Square Window. **c)** Binarized Image with aLuminous Edge At Retinal Rim **d)** Binarized Image with Reflected Locations

The splendid periphery at the retinal edge, as seen in Figure 7a, arises while the patient struggles to place the human eye precisely on the image of the recording hardware and the surrounding illuminations at the sides of the eye. Figure 7b shows the case of gleaming cloud-like patches over the macular locale created by the illusion of light from the optical fundus, which is a frequent wonder in more young patients. In the proposed heuristic technique, the periphery is removed by the initial discovery of the width of the retinal edge within the image. By applying the Otsu threshold [21] to the image, this is achieved. Otsu's binarization technique expects the image after a bi-model histogram to consist of only two groups of pixels (front area and foundation). The most acceptable limit value, which can sort all pixels into two classes, is defined adaptively. It turns the retina into a white plate to a large degree and leaves the base black. The centre and radius of the retina are calculated using this yield. A spherical curtain with a circle, not necessarily a retinal ring, is created and attached to the first image for editing and maybe disposing of the periphery. While Otsu is short on the precision of precisely dividing the fundus area, it nevertheless offers an easy and mechanised approach to the calculation of rough fundus measurements for trimming unwanted curiosities on the edge.

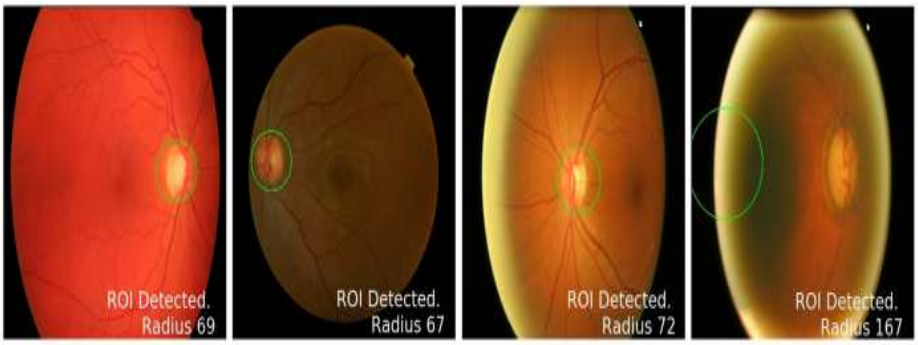

Figure 8 Outcomes of Heuristic Localization of OD. Subfigure 8d illustrates the Only Instance in Which Heuristic Was Unsuccessful. **a)** Accurate Localization of HRF image **b)** Accurate Localization of CFI& OCT image **c)** Accurate Localization of ORIGA Image **d)** The Only inaccurate Localization of ORIGA Image

The resulting image is then used by a customised adaptive binarization with an edge for each image as the average of the top 1% of the most beautiful pixels. This technique is used to find the hypothesised nucleus of OD. Before the focal point of this tough OD was established, morphological disintegration procedure was used to eliminate small, knowledgeable areas and sporadic motivational commotion. This is followed by a behavioural uptick to equate distinct white patches with less and more associated masses. The product of these tasks is a higher OD estimate. The centre and radius of this speculated disc location are then determined and the radius float, which is more visible than the determined set, is drawn to the image for the purpose of dividing and limiting the OD. These suggested positions will be physically checked by the master at the end of the day and critical adjustments will be made as necessary. Table 2.shows Intersection Over Union (IOU) of ground truth and heuristic calculations. The accuracy of the Test is measure of difference between Overlapping area and Union Area.

Table 2 IOU of Ground Truth and Heuristic Calculations

IOU%	20	50	60	70	80
Accuracy of Test	98.45	95.23	74.07	52.08	10.78

Table 3 Evaluation of IOU of Automated and Heuristic Techniques

IOU%	20	50	60	70	80
Heuristic Technique	98.45	95.23	74.07	52.08	10.78
Automatic Technique	99.99	99.99	99.99	98.25	93.78

6 Results of Heuristic Localization

The graphical assessment of the test and train data sets shows that the technique was unsuccessful with only three of the 573 (experiment + verification) images and only one of the 207 test images from three different data sets as shown in Figure 8. In order to test the precision of this method, IOU was computed between the bounding boxes offered by the manual ground truth and the proposed technique. Table 2 demonstrates the precision of this technique in accordance with the conflicting conditions between the present and the predicted disc. Results indicate that more than 95.1 per cent of ODs are grouped with more than 49.9 per cent of the actual disc in the projection. Also, almost 70% of the existing disc is used in 52 percent of the intended discs.

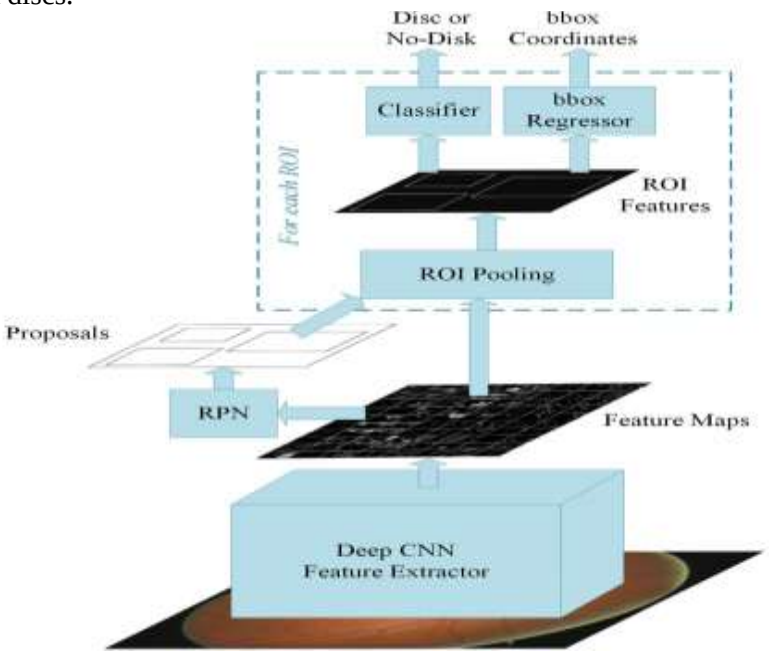

Figure 9 Internal Elements of Faster RCNN

The normal overlap between the ground truth and the predicted disc area for the test images is about 70%. It should also be remembered that the least possible IOU of the appropriately positioned disc in this technique is greater than 20%, while certain scientists [22-25] decided to consider its exact location if the discrepancy between the actual and predicted disc centre is not greater than the estimated disc thickness — if IOU > 0. Though the consequences of the heuristic-based approach are strongly optimistic, they are simple data sets and do not function well under real-life conditions in a

variety of fundus photographs. As a result, a fully automated methodology for precise disc localization was addressed in the following section without any realistic knowledge of data collection. Required changes are made to the explanations produced by the heuristic technique, and these semi-automatic interpretations have been given to the automatic localization methodology in accordance with the ground reality.

7 Two-Stage Technique for Automatic Classification and Disc Localization: the Proposed Method

After creating an essential GT for the training of automatic technique, now this part specifies a comprehensive result for robust and reliable localization of OD and its classification into glaucomatous or healthy.

7.1 Automatic Disc Localization

Present approaches used data sets and their experimental understanding of data sets for disc localization. In this analysis, the fully automatic localization is suited to the faster RCNN[26-28], which is connected to the network for the position of the object. As seen in Figure 9, the model contains of three important modules: RPN (Region Proposal Network), Bounding Box Regression, and CNN Classifier. RPN makes a number of irregular rectangular article suggestions for associated objectless ratings. These proposals are submitted to CNN, who shall arrange whether the report in question is available in the proposal. At that point, to customise the square shape near the object and to provide the exact region of the object in the picture, the Bounding Box Regression is carried out. The results of the faster RCNN disc localization on the three data sets given in Table 3 are described in Table 1. From Table 3, the faster RCNN offers 100 % accurate position for 60 percent IOU and a standard 96.10 percent overlap over the following three data sets. The effects of the mechanised position on the various data sets and the thorough analysis of these can be seen in the results area.

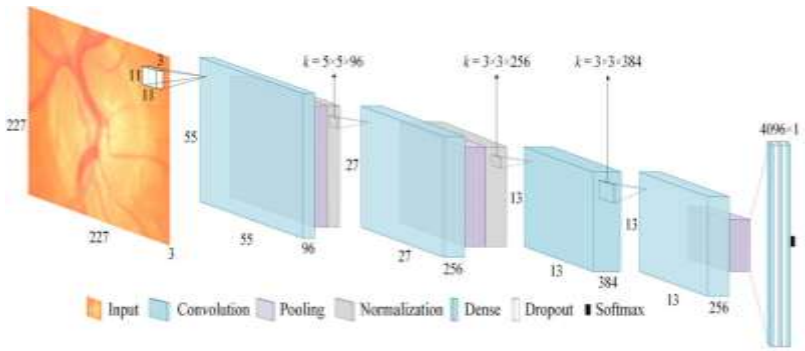

Figure 10 CNN Utilized for Classification of Glaucoma

Table 4 Efficiency of Automatic Disc Localization Algorithm on an Invisible Data Set

Algorithms	Messidor N = 1250	DRIONS-DB N = 110	DRIVE N = 45	DIARETDB1 N = 90	Criterion (IOU >)
Proposed (RCNN-based)	98.15	98.19	96.45	99.99	50
Machine Learning (ML) techniques	98.92	-	86.00	-	0
SVM Techniques	98.01	-	-	93.78	0

7.2 Glaucoma Classification

In the key step, OD is collected since a significant portion of glaucoma associated data is enclosed in this region [5, 6]. Extricating this ROI not only creates a mathematically efficient smaller introduction image, but also allows deep NN to zero in the most significant aspect of the image. The CNN prototype used in this analysis is shown in Figure 10. Four convolutionary layers have been used in the network aided by three fully related layers. Max pooling with covering phases and nearby reaction standardisation was used after the initial two convolutionary layers. In addition, the fourth convolutionary layer is accompanied by Max Pooling. The original two fully related layers are monitored by drop-out layers with a drop-out rate of 0.6. The performance of the last thick layer is forwarded to the SoftMax feature, which provides all grade expectations.

7.3 Convolutional Layers

From a significant level viewpoint, convolutionary layers are taken to take significant highlights from an image. The layers at the beginning of the network seem to grasp simple highlights such as bends, corners, and shapes, while the subsequent layers study more complex and special highlights are ears and hands. Numerically, this is achieved by first using a kernel or a size m × m detector function, by sliding it to the information space, and by convolution between the bit and the information fixed at all point. Usually,

the scope of the part is slighter than the input space. However, the depth of the component must be equal to the depth of the details. Each convolutionary layer uses different parts to secure spatial measurements more easily. Each part of the information space searches for a specific component and generates a map element. In Figure 10, 96 portions of each scale 11 x 11 x 3 are used by the initial convolutionary sheet. As a convolution is a straight-line process (component informative repetition of portion and info-fixing values followed by their aggregate), playing out different convolutions in multiple layers winds up in one key direct action and reduces the network's learning capacity along these lines. The output of each convolutionary layer is passed through a nonlinear function to solve this problem.

ReLU (Rectified Linear Unit), characterised as f(y) = max (0,y), is the greatest prominent nonlinear function utilized to create the nonlinear features of the network.

Table 5 Complete Performance Methods of CNN Classifier Utilizing Random Training

Category	Accuracy(%)	Recall (%)	F1-Score	No. of Images
Glaucoma	68.57	34.53	0.4625	130
Healthy	82.12	95.9	0.9647	413
Total	78.21	80.67	0.8955	550

7.4 Normalization Layers

The LRN (Local Response Normalization) layer is the scientific equivalent of horizontal neural repression that reflects the ability of an enthusiast neuron to regulate its neighbours. The LRN is used to stabilise it across the local vicinity of these excited neurons, as the activation of ReLU may be boundless for those neurons. This causes a rivalry between neuron outputs for critical events, which is decided by a variety of kernels and facilitates better generalisation.

7.5 Pooling Layers

Pooling layers are used without losing any notable information to download sample element maps. This is accomplished by holding from each section of the highlight guide a small window of size p x p and giving, for instance, a regular approximation of that window. The window would then slide over the entire map of the component with the pixel process. At the point where p > s is hit, overlapping pooling is accomplished. Not only does it minimise the magnitude of the feature diagram, it also promotes the control of over-fitting, which is a big problem in deep networks with limited data sets. In our method, Max Pooling was used to pick the biggest reward from the frame, with a step of 2 pixels and a window size of 3×3.

7.6 Dropout Layers

In addition, drop-out layers are helpful during preparation to block overfitting and aid speculation. By measuring the yields of hidden neurons equal to '0' with the likelihood given, this layer is carried out. In this way, the new training pass would not incorporate these recycled neurons. The network is ordered to learn extra vigorous highlights in much the same way. A dropout likelihood equal to 0.5 is used by the network in Figure 10.

8 Results and Discussion

This part details and investigations the consequences of classification and localization phases described.

8.1 Results of Automated Disc Localization

The model was prepared for 100,000 emphases using VGG16 as a pre-prepared classifier for Pascal VOC2007 for computerised OD localization [21]. The GT created by our semi-automated technique is used alongside 573 photographs, recently used to test and train the heuristic strategy, to prepare the network. The consequence of the computerised methodology for the localization of the circle is seen in Table 3. When prepared and analysed on the CFI & OCT, ORIGA, and HRF data sets, on other widely available information bases, the model has already been tested and results are compared, and some of the best in class approaches have been explicitly adapted for these data sets. The findings feature a near-presentation of fully mechanised methods with modern heuristic calculations. The precision of our strategy is half IOU. The findings set out in [22-25] are for IOU > 0 while the others have also found position correct if half of the coverage is reached. As can be seen from Table 4, the projected strategy is basically performed in a manner that is equivalent to the current heuristics techniques, which suggests that it has the ability to learn a discriminatory representation of OD. It should be noted that for a specific data set in the centre, heuristic strategies are typically prepared.

Figure 8 and Figure 11 indicate that there are generous varieties of resolution, contrast, brightness and colour, and so on between images of different data sets. The predicted fully automated strategy was not prepared on any of the two data sets recorded in Table 4, but then prevalent than those techniques precisely suited to those particular data sets. The average overlap between real and expected OD bounding boxes is 84.82 % for MESSIDOR, 80.46 % for DRIONS-DB, 84.13 % for DRIVE and 84.65 % for DIARETDB1.

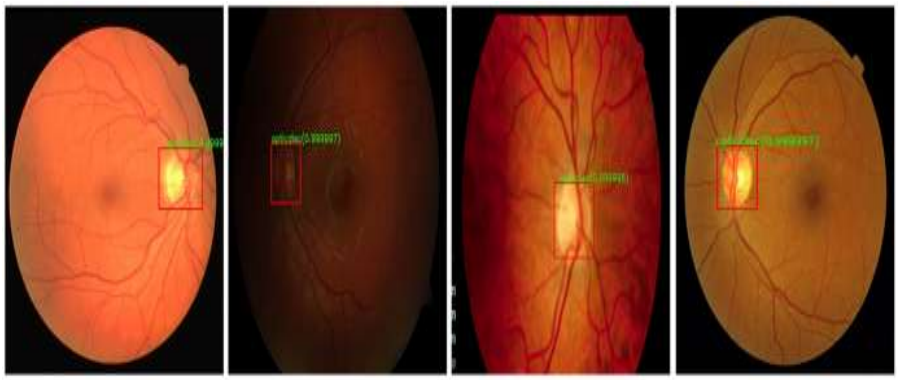

Figure 11 Results of Automatic Localization on different data sets. Note the Contrast and Illumination Differences among the Data Sets. **a)** Test Image from DRIVE **b)** Experimental Image from DIARETDB1 **c)** Test Image from DRIONS-DB **d)** Test Image from Messidor

8.2 Results of Classification

A separate inspection technique is carried out in the ORIGA data collection, as seen in Table 1, where it is assured that a subset of the glaucoma photos is used in each training cluster. This technique is used to avoid any predisposition to a healthier group. In comparison, a constant learning pace of 0.0001 alongside Cross-Entropy and Adam analyzer failure was used during preparation.

8.2.1 Results with Random Training

As no specification splitting of the test and train set is required for this data set, in comparison to the proposed model and other late-announced work, we have previously used identical training arrangements used by the vast majority of them [4, 5 , 7, 13,15]. In this analysis, the model has been proposed over and over again, each time haphazardly taking 99 images for preparation and remaining for research. Out of more than 1500 training passes the finest mixture of test and train break has caused in an average order precision of 78.97 per cent. For the aggregation of unequal data sets, such as ORIGA, where the number of images in the two divisions is greatly lopsided, as seen in Table 1, precision only does not reflect the true execution of the classifier. Additionally, other execution metrics such as precision, analysis, and F1-score are considered in this manner. Accuracy shows the proportion of the correct assumptions of all the predictions complete by some classifier for a given class. Examination or affectability, then again, defines the portion of the proper prediction for a category out of a true absolute number of tests in that course. F-score is the consonant mean of both

precision and analysis and offers a bound together metric to determine the presentation of the classifier. Numerical effects of all of these performance metrics are given as

$$Precision = \frac{TruePositives}{TruePositives + FalsePositives} \quad (1)$$

$$Recall = \frac{TruePositives}{TruePositives + FalseNegatives} \quad (2)$$

$$F1\text{–}Score = 2\frac{Precision \times Recall}{Precision + Recall} \quad (3)$$

Table 5 lists the Class-based average accuracy, F1 and recall ratings. Figure 12 indicates the matrix of uncertainty. Figure 12 reveals that out of 412 safe images, 21 are misclassified as having glaucoma, and 391 are specifically identified. Instead, only 48 of 91 glaucoma images are imperfectly categorised and a total of 139 glaucoma images are correctly classified as stable.

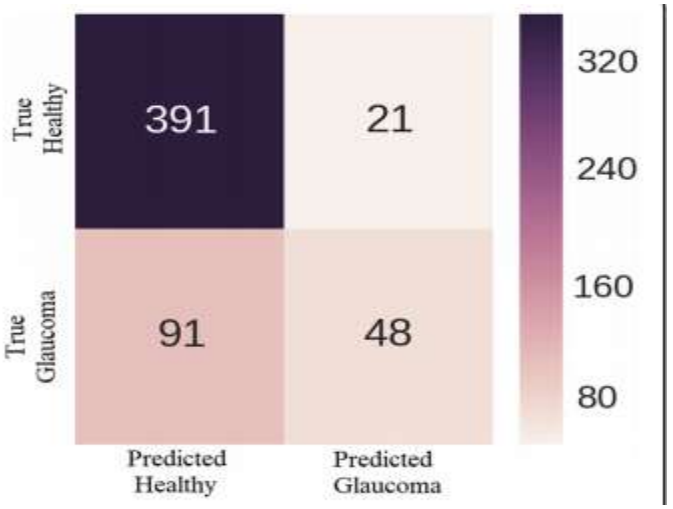

Figure 12 Confusion Matrix Demonstrating Dissemination of False Positives, False Negatives, and True Positives

The ROC (Receiver Operating Characteristic) curve was a common performance metric taken to test the discriminating capabilities of binary classifiers. It customs a different threshold, provided that the example is beneficial, to measure the overall efficiency of the classifier by preparing sensitivity (recall) versus specificity. TNR (True Negative Rate) or Specificity as defined

$$Specificity = \frac{TrueNegatives}{TrueNegatives + FalsePositives} \quad (4)$$

The AUC of this ROC offers a statistical measure to evaluate the presentation of dissimilar classifiers. Table 6 reveals the predominance of our paradigm in other related educations as far as AUC is concerned. As the majority of the everything referred to in Table 6 declared AUC as success indicators for their classifiers, it was observed that for some mixtures of 551 test and 99 train images, our model had the option of achieving higher AUC, 87.8%, than five results in [4,5, 7, 13,15] while anticipating only a healthy class for each test image, offering a strong class analysis. It means that the balance between the affectability and the explicitness of the models will lead to higher AUC without being held back by anything. As a result, without a well characterised test and train break and without understanding the degree of glaucoma and stable images in both sets, AUC actually cannot represent the overall and accurate picture of the classifier. Other execution figures, such as precision, re-examination and f-scores, must also account for a fair re-examination and an exhaustive association with various models. Not withstanding the incidence of all around the characterised test and train break, AUC alone may be adequate to quantify the grouping capacity of the model.

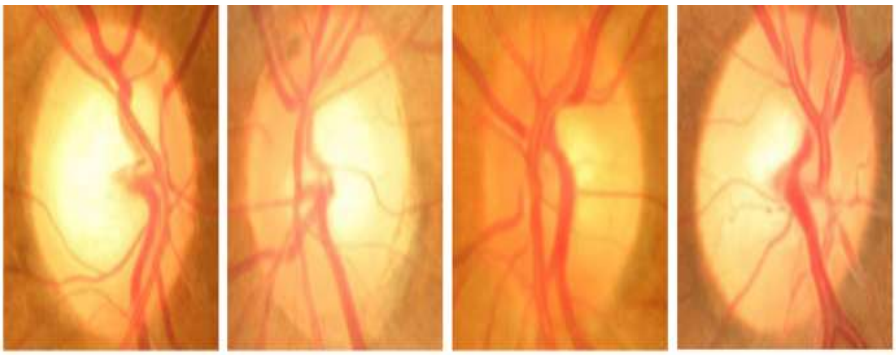

Figure 13 Samples of Incorrect and Correct Classification of Glaucoma Utilizing DCNN. **a)** Accurately Classified Glaucoma **b)** Improperly Classified Glaucoma **c)** Accurately classified Healthy image **d)** Improperly Classified Healthy Image

Table 6 Evaluation of Acquired AUC with Current Modern Methods Utilizing Random Training

Performance measures	[4]	[5]	[7]	[13]	[15]	Proposed Technique
AUC	0.842	0.848	0.848	0.848	0.852	0.878

Table 7 Complete Performance Measuring of CNN Classifier Utilizing Cross-Validation

Class	Accuracy (%)	Recall (%)	F1-Score
Glaucoma	65.52 ± 6.65	43.66 ± 4.95	0.5231 ± 0.534
Healthy	82.31 ± 2.88	91.86 ± 2.29	0.8681 ± 0.246
Total	78.97 ± 3.78	79.49 ± 3.24	0.7788 ± 0.366

8.2.2 Results with Cross-Validation

Recognizing this effect in the presentation appraisal of the classifiers, and 10-fold cross-validation of the data collection was carried out to support prospective investigators in the thorough evaluation of their models. The data set was haphazardly isolated into 10 equivalent sections. In one training course, for example, the original section is used for study and an additional nine are used for training. Later, for example , the second portion is saved aside for analysis, and the other nine are used for preparation. Normal is believed to monitor more than 10 training sessions and the collective test accuracy is calculated to be 79.49 per cent ± 3.24 per cent.

F1 ranking, recall, and class-based accuracy are set out in Table 7. The association of AUC using cross-approval with different works is summarised in Table 8 which indicates that the preferred network beats the specifics of the craftsmanship findings for glaucoma classification in the ORIGA data collection. Figure 13 displays the test images of effectively and wrongly clustered stable and glaucoma images.

Table 8 Evaluation of Acquired AUC with Current Modern Techniques Utilizing Cross-Validation

Performance measures	[4]	[5]	[7]	[13]	[15]	Proposed Technique	
						Random Training	Cross-Validation
AUC	0.842	0.848	0.848	0.848	0.852	0.878	0.887
Sensitivity (%)	N/A	N/A	N/A	68	N/A	79	79.14

In addition, an improvement in data was also made in order to analyse the implications for the consistency of the arrangement. From four corners and a focal point of 256 × 256 × 3 OD-extricated prints, vertical and horizontal flips and 227 × 227 × 3 patches were made. However, the analyses carried out without and with knowledge extension did not reveal any important difference between the presentations of the two methodologies. Similarly, the effect of the multifaceted existence of the network on the accuracy of the arrangement was investigated. For this function, Alexnet] is used as a reference model and surveys the impact of the quantity of layers

on the output of the network, given that a wide variety of different conditions are equal. It was shown that the extension of the multi-faceted existence of the network decayed the accuracy of the classifier. The purpose behind this corruption efficiency may be the restricted reach of the data collection. During preparation, a deeper network shaves the potential for over-fitting when inadequate training assessments are carried out. The networks are performing in a manner that is superior to the others with four convolutionary layers. The best performing pattern between all the modifications attempted is used for classification and is the one seen in Figure 10.

9 Conclusion

In this study, a two-phase response to OD classification and localization was suggested for diagnosis of glaucoma. Understanding that OD helps examine the eye for a number of conditions like glaucoma, this analysis used a fully computerised disc localization strategy that is based on faster RCNN. This methodology dispenses with the necessity to improve data set-explicit observational or heuristic localization techniques by offering reliable and robust localization over an expansive spectrum of data sets. The presentation of this entirely mechanised system sets new best in class gives about 6 out of 7 publicly available data sets with IOU more than half of them. The order of pictures in ailing and solid use of CNN has also been examined. While certain scientists have detailed about 95 percent exactness on private data sets or have painstakingly selected a limited collection of images from publicly available data sets, the characterization precision and the ROC AUC for readily accessible ORIGA data sets have sought to increase. Although higher AUC is dramatically obtained for ORIGA with both cross-validation of k-fold and random training, the full presentation evaluation of the classifier reveals that the network has difficulty learning biassed characteristics to categorise glaucoma images in this publicly available data collection. The fine-grained discriminatory data in the pictures of this data collection has been lost due to the growth of the network hierarchy. As a result , additional effort is required to configure a few classifiers fit for reliable glaucoma image recognition.

References

[1] Abràmoff MD, Garvin MK, Sonka M.. “Retinal imaging and image analysis”, IEEE Rev Biomed Eng.Vol.3, pp.169–208. 2010.

[2]Siddalingaswamy P, Prabhu KG., “Automatic localization and boundary detection of optic disc using implicit active contours”, Int J Comput Appl. Vol.1, no.6, pp.1–5. 2010.

[3]Harangi, B., Qureshi, R.J., Csutak, A., Peto, T., Hajdu., "Automatic detection of the optic disc using majority voting in a collection of optic disc detectors", IEEE international symposium on, pp. 1329–1332,2010.

[4]Kovacs, L., Qureshi, R.J., Nagy, B., Harangi, B., Hajdu.A., Graph based detection of optic disc and fovea in retinal images", 4th International workshop on. IEEE, pp. 143–148, 2010.

[5]Goatman KA, Fleming AD, Philip S, Williams GJ, Olson JA, Sharp PF., "Detection of new vessels on the optic disc using retinal photographs", IEEE Trans Med Imaging, Vol.30,no.4, 972–979,2011.

[6]Liu, J., Wong, D., Lim, J., Jia, X., Yin, F., Li, H., Xiong, W., Wong, T.: "Optic cup and disk extraction from retinal fundus images for determination of cup-todisc ratio", Industrial electronics and applications, 3rd IEEE Conference on Industrial Electronics and Applications, pp.1828–1832,2008.

[7] Nyúl LG., "Retinal image analysis for automated glaucoma risk evaluation", Proceedings of SPIE - The International Society for Optical Engineering, pp.7497:74971, 2009.

[8]Cheng S-C, Huang Y-M., "A novel approach to diagnose diabetes based on the fractal characteristics of retinal images", IEEE Transactions on Information Technology in Biomedicine, Vol.7, no.3, pp.163–70, 2003.

[9] Abbas Q., "Glaucoma-deep: detection of glaucoma eye disease on retinal fundus images using deep learning", Int J Adv Comput Sci Appl., Vol. 8,no.6, pp.41–45,2017.

[10] Mookiah MRK, Acharya UR, Lim CM, Petznick A, Suri JS., "Data mining technique for automated diagnosis of glaucoma using higher order spectra and wavelet energy features", Knowledge-BasedSystems, Vol.33, pp.73–82,2012.

[11]Bengio Y, Courville A, Vincent P., "Representation learning: a review and new perspectives", IEEE Trans Pattern Anal Mach Intell. Vol.35,no.8.pp.1798–828,2013.

[12]Eswaran C, Reza AW, Hati S., "Extraction of the contours of optic disc and exudates based on marker-controlled watershed segmentation", Computer science and information technology, Vol. 8, pp. 719–723,2008.

[13]Chràstek R, Wolf M, Donath K, Michelson G, Niemann H., "Optic disc segmentation in retinal images", Bildverarbeitung Für die Medizin , pp. 263–266,2002.

[14]Dashtbozorg B, Mendonça AM, Campilho A., "Optic disc segmentation using the sliding band filter", Comput Biol Med., Vol. 56, pp. 1–12, 2015.

[15]Kobatake H., "A convergence index filter for vector fields and its application to medical image processing", Electron Commun Jpn, Vol. 89, no. 6, pp. 34–46, 2006.

[16]Samanta, S., Saha, S.K., Chanda, B., "A simple and fast algorithm to detect the fovea region in fundus retinal image", Emerging applications

of information technology (EAIT)", 2nd international conference on Emerging Applications of Information Technology, pp. 206–209, 2011.
[17]Zhang D, Zhao Y., "Novel accurate and fast optic disc detection in retinal images with vessel distribution and directional characteristics", IEEE J Biomed Health Inform, Vol. 20, no. 1, pp. 333–342, 2016.
[18]Mary MCVS, Rajsingh EB, Jacob JKK, Anandhi D, Amato U, Selvan SE., "An empirical study on optic disc segmentation using an active contour model", Biomed Signal Process Control, Vol. 18, pp. 19–29, 2015.
[19]De La Fuente-Arriaga JA, Felipe-Riverón EM, Garduño-Calderón E., "Application of vascular bundle displacement in the optic disc for glaucoma detection using fundus images", Comput Biol Med, Vol. 47 pp. 27–35, 2014.
[20]Ahmad H, Yamin A, Shakeel A, Gillani SO, Ansari U., "Detection of glaucoma using retinal fundus images", Robotics and emerging allied Technologies in Engineering (iCREATE), International Conference on Robotics and Emerging Allied Technologies in Engineering ICREAT, 2014.
[21] Zhang Z, Yin FS, Liu J, Wong WK, Tan NM, Lee BH, Cheng J, Wong TY., "ORIGA-light: an online retinal fundus image database for glaucoma analysis and research", IEEE annual international conference of the Engineering in medicine and biology society (EMBC), pp. 3065-3068, 2010.
[22]Canny J., "A computational approach to edge detection", IEEE Transactions on Pattern Analysis and Machine Intelligence, Vol. 8, no. 6, pp. 679-698, 1986.
[23]Li A, Cheng J, Wong DWK, Liu J., "Integrating holistic and local deep features for glaucoma classification", 38th annual international conference of the Engineering in medicine and biology society (EMBC), pp. 1328–1331, 2016.
[24]Akyol K, Şen B, Bayır Ş., "Automatic detection of optic disc in retinal image by using keypoint detection, texture analysis, and visual dictionary techniques", Computational and mathematical methods in medicine, 2016.
[25]Simonyan K, Zisserman A., "Very deep convolutional networks for large-scale image recognition", Computer Vision and Pattern Recognition, 2014.
[26]Al-Bander B, Williams BM, Al-Nuaimy W, Al-Taee MA, Pratt H, Zheng Y., "Dense fully convolutional segmentation of the optic disc and cup in colour fundus for glaucoma diagnosis", Symmetry, Vol. 10, no. 4, 2018.
[27]Ho TK., "Random decision forests", Document analysis and recognition, Proceedings of the third international conference on, vol. 1, pp. 278–82. 1995.

[28]Mary MCVS, Rajsingh EB, Naik GR., "Retinal fundus image analysis for diagnosis of glaucoma: a comprehensive survey", IEEE Access, Vol. pp. 4327–4354, 2016.

[29]Khalil T, Khalid S, Syed AM., "Review of machine learning techniques for glaucoma detection and prediction", Science and information conference (SAI), pp. 438–42, 2014.

Biographies

R. Anandh ,Research Scholar, Department of CSE, FEAT, Annamalai University, Chidambaram, Tamil Nadu, India.

G. Indirani, Associate Professor, Department of CSE, Government College of Engineering, (Deputed from Annamalai University) Bargur, Tamil Nadu, India.